



## Research Article

Paper presented in the special issue of [Advanced Materials in Additive Manufacturing]

# Web Stiffening of Additive Manufactured Polylactide (PLA) Railroad Tracks Using Fiberglass Wrapping

Navanit Sri Shanmugam<sup>1\*</sup>, Vidya Subhash Chavan<sup>1</sup>, David Boyajian<sup>2</sup>, Shen-En Chen<sup>1</sup>, Nicole L. Braxtan<sup>1</sup>, R. Janardhanam<sup>1</sup>

<sup>1</sup>Department of Civil and Environmental Engineering, University of North Carolina at Charlotte, Charlotte, NC, USA

<sup>2</sup>Department of Civil Engineering and Construction Management, California State University, Northridge, Northridge, CA, USA

E-mail: [nshanmug@uncc.edu](mailto:nshanmug@uncc.edu)

**Received:** 8 June 2023; **Revised:** 8 August 2023; **Accepted:** 8 August 2023

**Abstract:** Three-dimensional (3D) printed railroad tracks can properly address the rendering of a variety of topographic profiles of naturally occurring landscapes and reduce construction costs. Load tests of PLA railroad tracks found that web failure is a dominant failure mode. This paper evaluates the web stiffening strategies of additively fabricated PLA railroad tracks for rail-guided, micro-people movers (MPMs). To strengthen the track web, web-widening with additional PLA material and stiffening using composite reinforcement using glass fiber reinforced polymer (GFRP) wrap have been investigated. The composite wrapping technique was conducted by bonding fiberglass cloth to both sides of the web using a polymeric resin. Flexural load tests were conducted on the specimens with different infill volume percentages. A linear trend was observed on the peak bending capacities of specimens with PLA infill fiber contents ranging between 20% to 100%. Different failure modes were observed for the different percentage specimens during the tests. When compared to their unreinforced counterparts, the 60% infill specimen had the largest increase in strength about 1,500 N in bending with the addition of GFRP wrap. The tangent stiffnesses of all samples were calculated which showed the 100% infill specimen had the highest increase of approximately 50%. The wrapping reinforcement was found to significantly modify the failure mechanisms of the 3D-printed tracks with different infill volume percentages. The strengthening of the 3D-printed tracks using GFRP wrapping is also shown to be similar to the widening of web sections of the additively printed railroad tracks.

**Keywords:** 3D printing, fiber reinforced polymer (FRP) composite fiberglass wrapping, MPMs, bending flexure tests, experimental investigations

## Nomenclature

3D	Three-dimensional
3DCP	Three-dimensional concrete printing
AM	Additive manufacturing
CAD	Computer-aided drawing
FRP	Fiber reinforced polymer
GFRP	Glass fiber reinforced polymer

Copyright ©2023 Navanit Sri Shanmugam, et al.

DOI: <https://doi.org/10.37256/dmt.3220233190>

This is an open-access article distributed under a CC BY license  
(Creative Commons Attribution 4.0 International License)

<https://creativecommons.org/licenses/by/4.0/>

MPMs	Micro-people movers
PLA	Poly lactide
RC	Reinforced concrete
SLS	Selective laser sintering
UTM	Universal testing machine
UV	Ultraviolet
VIP	Vacuum infusion process

## 1. Introduction

3D printing or AM is generative and has the advantages of rapid prototyping and flexibility toward the manufacturing of complex designs. The typical workflow for 3D printing involves first creating a design of the envisioned part(s) using CAD software, which is then transferred to a 3D printer for the actualization of the desired product [1, 2]. This additive technology is accomplished layer by layer [2] to minimize energy and material wastage which serves in rendering a more sustainable product for onsite construction needs [1, 3]. On this latter point, one of the ways to reduce material waste is by determining the optimal density as a function of the print layer needed to carry out the defined functionalities of the material.

3D printing of railroad tracks offers an unusual but logical choice because of the flexibility introduced to design track layouts on complex terrains [4]. More recently, 3D printing using laser powder deposition has been applied for track repairs [5]. Chen et al. [6] suggested using the 3D printing technology for onsite railroad track production, which has the advantage of minimizing the amount of earthwork required for customizing terrain constraints for traditional mill-manufactured tracks. It was demonstrated that this approach is a feasible way of producing 3D printed (7½ inch 190.5 mm) railroad tracks for guided MPMs. Figure 1 shows an electric MPM running on a typical 190.5 mm gauge track. By performing mechanical tests, the authors were able to show that the printed material densities can dictate failure modes and the resulting mechanical strengths of the railroad tracks.



**Figure 1.** The electric MPM: (a) the MPMs; (b) fixed-axis bogie

Conventional manufacturing typically consists of material removal processes like machining and plastic forming processes through hot or cold rolling techniques. As suggested by the name, AM (a.k.a. 3D printing) produces materials through the deposition or addition of the material layer-by-layer until the desired part or structure is realized. This technology is initiated by creating a design in a CAD environment that is then sent to a 3D printer for the protrusion of the desired element [7, 8]. One of the advantages of producing a part through a layer-by-layer building-up approach is the savings in material afforded as sharply contrasted to parts produced through subtractive technologies [9]. Advances in AM technologies have even enabled construction using various materials such as ceramics [10], concrete [11], and steel structures [12]. Regarding the latter, steel construction can benefit from laser powder technology, wire

arc automated welding, and the subtractive manufacturing process of laser melting. As for the most widely used construction material, 3DCP mix design has far-reaching applications. Finally, revolutionary strides are being made with more advanced techniques such as stereolithography, which involves a photopolymerizable suspension cured by a UV laser, and the SLS approach involving melted powders resulting from the use of lasers as well. Both techniques have been applied to ceramics and metals.

FRPs are corrosion-resistant, lightweight, and have high strength, high elastic modulus, and high resistance to environmental factors. FRP materials consist of two basic materials: The fiber and the matrix. The varieties of fibers used in such composite materials typically include glass, carbon, basalt, and aramid. The matrix materials consist largely of resins of the epoxy, vinyl ester, or polyester types. Epoxy resin adhesives are used to bond FRP cloth to surfaces, and being that they are thermosetting polymers, the working environment should be below that of the glass transition temperature, otherwise a significant reduction in strength, stiffness, and bonding properties will result [13, 14].

Over the past several decades, extensive research has been conducted on the strengthening of RC structures using externally bonded FRP laminates, which has been shown to improve the flexural and shear capacities of various RC components externally [15-20]. The behavior of FRPs for the strengthening of other materials such as wood [21-23] and steel has also received considerable attention [24, 25].

Currently, metal-based (brass, steel, or aluminum) rail tracks in either straight or curved formations, are the most common in the construction of MPMs. However, for optimal flexibility characteristics to best accommodate naturally occurring landscape settings (i.e., topographical effects), and to minimize possible electromagnetic field interferences due to underground cables and powerlines, 3D printed rails offer an attractive alternative to their more traditionally formed counterparts. Depending on whether the placement of the track is on a slab or a tie type of support, the load-bearing capacity becomes an important factor for load transfer between the track and rail seat which may, in turn, result in the members experiencing flexural or compressive stresses.

The MPM displayed in the following pictures utilizing an electric locomotive car moving upon a pair of 190.5 mm gauge aluminum tracks (Figure 2), imparts loads onto these members from its chassis, bogies, motor, brakes, controller, and a power source. A bogie is a frame that carries the vehicle and is supported by a suspension system connected to the axles and the wheels which are locked upon a solid axle to prevent them from turning at different speeds.



**Figure 2.** Conventional aluminum railroad track for MPM

The locomotive does not have brakes and relies on friction in the motor to slow down, which can add stress to the railroad tracks. Figure 1 shows the locomotive and Figure 2(b) shows a closeup of the fixed-axis bogie running on the aluminum tracks. The total self-weight of the locomotive section of the MPM (as shown in Figure 1(a)) is about 226.8 kg (500 lb).

Regardless of the technique being employed, proper material characterization is the first step before such technologies can confidently be utilized in engineering applications. To minimize the usage of materials, PLA tracks were printed at different infill volumes ranging from 20% to 100%. Load tests have shown that web failure was the

primary cause of failure in a bending scenario, hence, to strengthen the tracks, FRP glass cloth was applied to the tracks and studied. This is a prevalent strategy adopted by the construction industry when externally reinforcing concrete structures [26-28].

## 2. Sample preparation and testing

### 2.1 3D printing of railroad track

The prototyping of the 3D printed PLA rail track consists of the production of 100 mm long beams that were produced with 3.175 mm diameter grooves in the top and bottom flanges for future sensor placements [6]. Figure 3 shows the CAD diagrams of the PLA rail track prototype where the web width is 3.40 mm, the top, and bottom flanges have widths of 10.67 mm and 19.05 mm, respectively, and the height of the member is 25.4 mm. The moment of inertia ( $I_{xx}$ ) of this beam is  $12,212 \text{ mm}^4$ . The dimensions of the aluminum railroad track from Figure 2 were measured and replicated for the study. The tracks were 3D printed using a Flashforge Adventurer 3 Lite 3D printer with PLA filaments of diameter 1.75 mm.

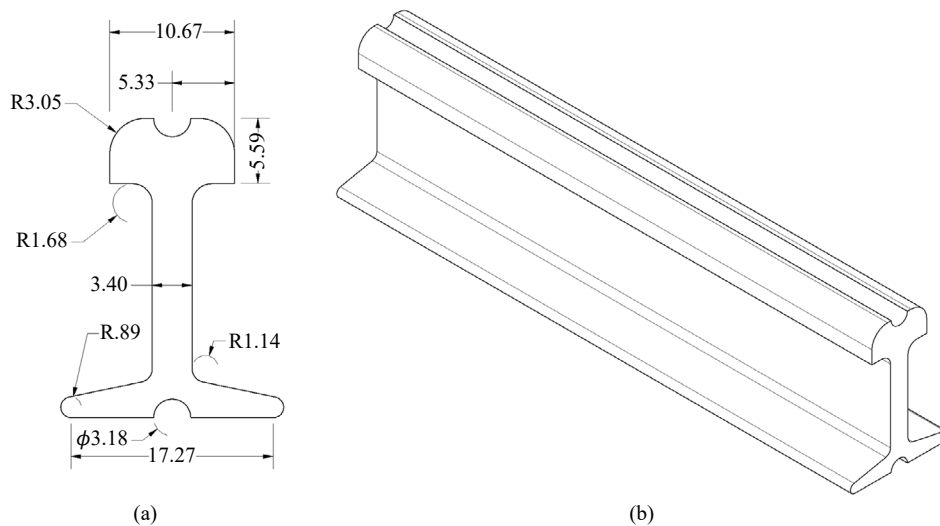


**Figure 3.** CAD diagrams of the track: (a) cross-section (dimensions in mm); (b) isometric view of the specimen

The process involves the filament which gets passed through a heating liquefier that melts the thermoplastic. The Ultimaker CURA 4 software is programmed to slice the rail track model and directs the printer during the fused deposition process (FDP) that layers the plastics into the desired shape. The extruder has a nozzle diameter of 0.4 mm with a working temperature set at 210 °C and a forming bed temperature of 50 °C. Figure 4 shows the schematic of the fabrication process.

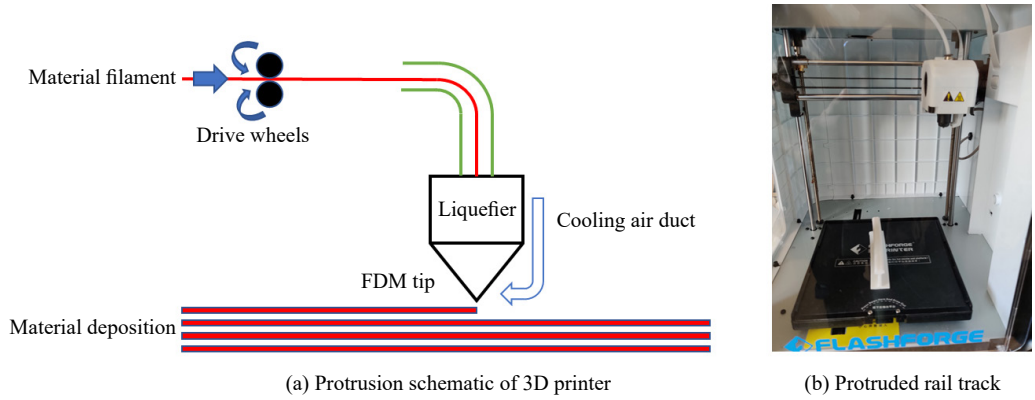


Figure 4. Railroad track fabricated through the fused deposition process

Specimens of 20%, 40%, 60%, 80%, and 100% PLA density were printed to determine the density effects on the mechanical properties. The 100% sample refers to a fully solid beam. Figure 3 shows a fully layered track and Figure 5(b) shows a partially printed web section with a 20% printed density. Lower-density samples have voids in them resulting from a smaller amount of PLA material used during the manufacturing process. As the track density was formed by a layering technique, the structural behavior is likewise dictated by both the layer directions and arrangements. A horizontal layering approach was used here since a vertical arrangement has been shown to result in lowered structural capacities [6]. Figure 5(a) shows an elevation view of a 20% track specimen that was formed by the horizontal layering technique.

Table 1 lists the test specimens, the PLA densities, fabrication duration, and the length amounts required of the 1.75 mm diameter PLA filaments used in producing those specimens during the fabrication process. Specimens with higher densities require more material and time to produce.

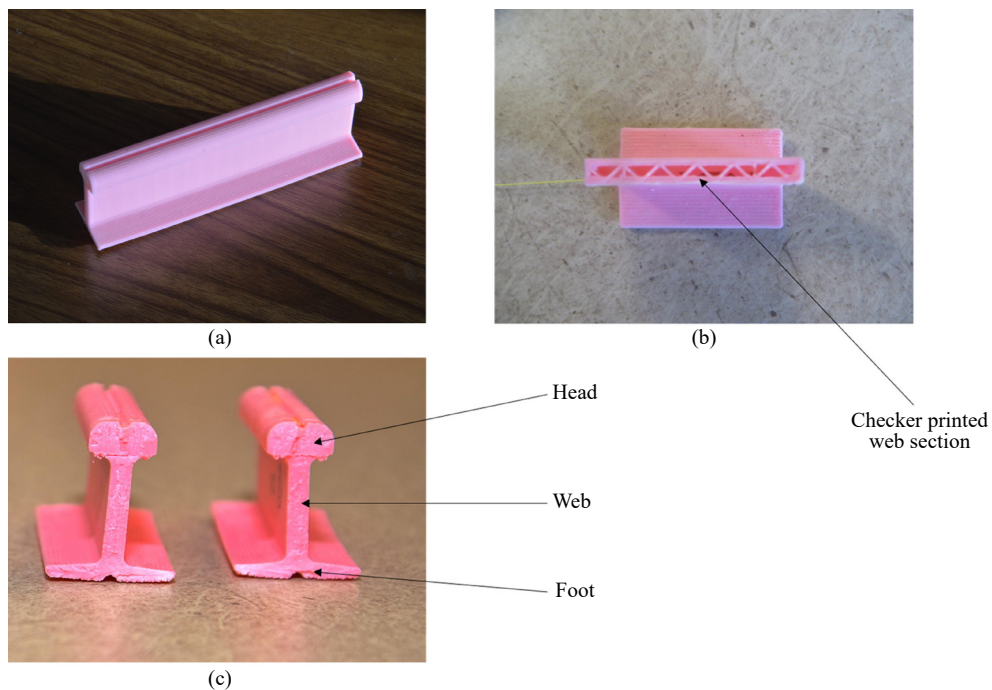


Figure 5. Exposed track sections with 20% fiber content showing: (a) flexural element; (b) hollowed web section checker printed; (c) fully printed cross section (100Flex)

**Table 1.** Fabrication duration and filament length for various specimens

Specimen name	PLA density	Fabrication duration (hours)	Filament length (m)
20FlexF	20%	3.0	5.86
40FlexF	40%	3.5	6.15
60FlexF	60%	4.0	6.44
80FlexF	80%	5.0	6.73
100FlexF	100%	6.0	6.99

## 2.2 Glass fiber reinforcement preparation

To enhance the performance of the 3D printed tracks, 0.2 mm thick fiberglass cloth (Figure 6) was used to externally reinforce the web on the rail tracks in this study. Strips of 60 mm × 17 mm 3M Bondo fiberglass cloth (P.N. 20128) were bonded to the midsection on both sides of the web, as shown in Figure 7. A 3M Bondo two-part epoxy (polyester resin and hardener, P.N. 20122) was used as the bonding agent (Figure 6(b)). The resin and hardener were thoroughly mixed in a container at a 100:1 ratio. This mixture was then applied to the mid-section (60 mm width) on the rail track web (Figures 7(a) and 8(a)). A piece of fiberglass cloth was then placed on the web surface (Figure 8(b)) with a coating of epoxy applied over the entire fiberglass strip (Figure 8(c)). A finished sample is shown in Figure 8(d). Table 2 shows the specimen types with peak load data.



**Figure 6.** (a) Fiberglass cloth; (b) resin-adhesive

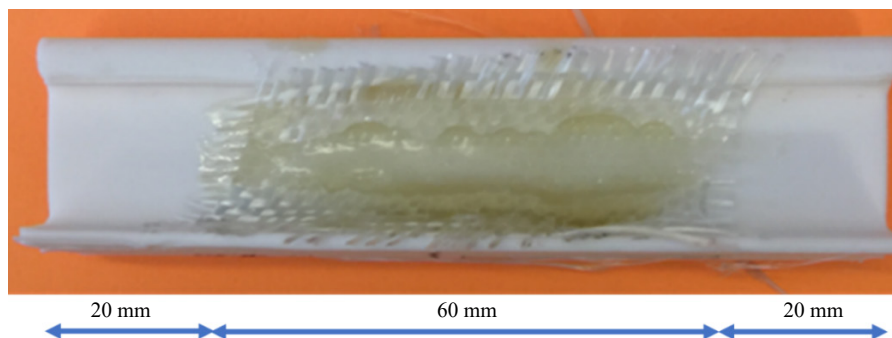


**Figure 7.** Fiberglass cloth bonded to the midsection (60 mm width) of the track web

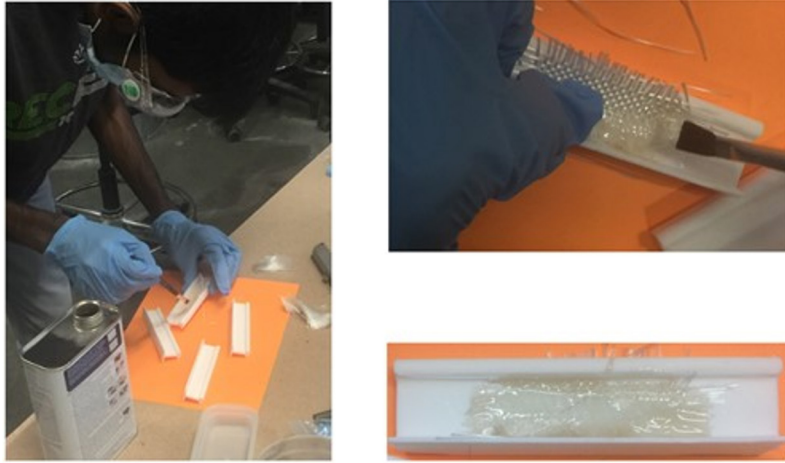


**Figure 8.** Rail track specimen wrapping preparation

**Table 2.** Loading at the peaks for different specimens

Specimen type	Peak 1 load (N)	Peak 2 load (N)	Peak 3 load (N)	Peak 4 load (N)
20FlexF	1,149.0	2,402.3	2,379.2	2,384.3
40FlexF	1,901.1	3,312.9	3,314.7	3,310.3
60FlexF	3,837.3	--	4,016.5	4,156.2
80FlexF	4,069.9	--	4,035.8	3,840.7
100FlexF	4,198.3	--	--	--

### 2.3 Flexural load test

To determine the wrapped sections' mechanical properties, a three-point bending test was performed to evaluate the flexural properties of the reinforced beams [29]. The load tests were conducted on a UTM as shown in Figure 9. Spacers were placed to make the sample lie within the traversing range of the UTM head. The test specimen was placed at the center of the loading area on top of steel supports (small bars) such that they are located 25 mm from the ends of the specimen. Another steel bar was placed at the mid-point above the specimen to transfer the load from the UTM head.



**Figure 9.** Flexural load setup

### 3. Results and discussions

#### 3.1 Failure mode profiling

The load versus displacement plots for the specimens are shown in Figure 10. The plots typically have multiple peak points of interest, which are visible for the 20%, 40%, and 60% specimens. In this study, the focus will be placed on the initial linear responses and the first peak load. Using the 20FlexF specimen in the way of illustration, the first peak point (1st peak load) corresponds to the first failure mode, which is the indentation of the loading head into the top flange of the specimen representing a failure of top fiber layers. The width of the indentation is 7.14 mm, which is close to the loading contact width of 6.35 mm. The next mode of failure is the localized buckling of the web along the longitudinal axis, which corresponds to the 2nd peak. Incidentally, the top flange was fully indented by this point in the experiment. Following this, delamination between the FRP wrap and the PLA track was found to occur at the 3rd peak. Finally, the fiberglass cloth was found to separate from the track and it was unable to carry any additional load at the 4th peak characterized by foot fracture (fiber rupture at the base of the beam). The typical failure modes including indentation, layer splitting, structural bending, debonding, and foot fracture are shown in Figure 11.

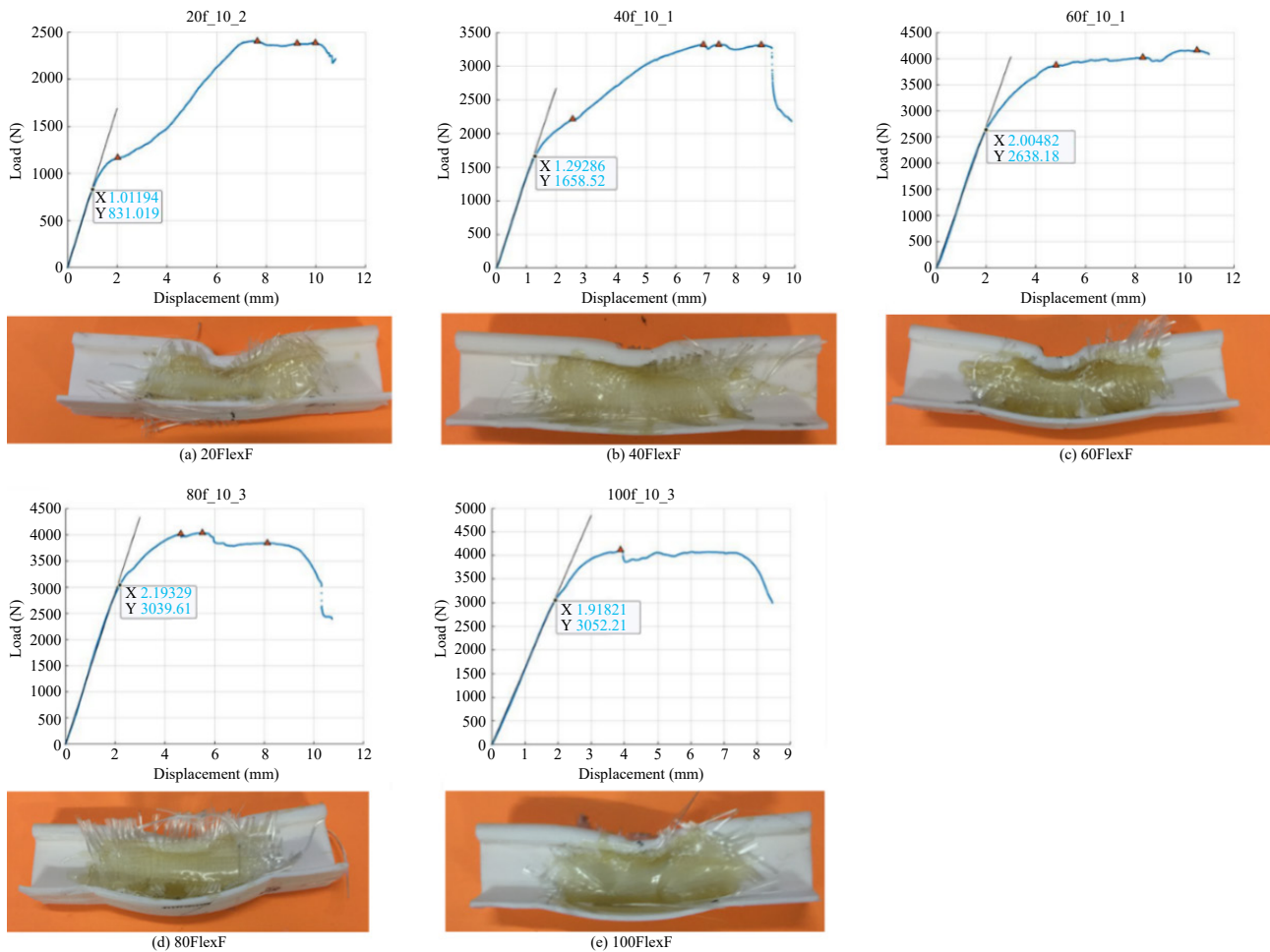


**Figure 10.** Load-displacement plots for fiberglass reinforced rail tracks with varying PLA percentages: (a) 20%; (b) 40%; (c) 60%; (d) 80%; (e) 100%



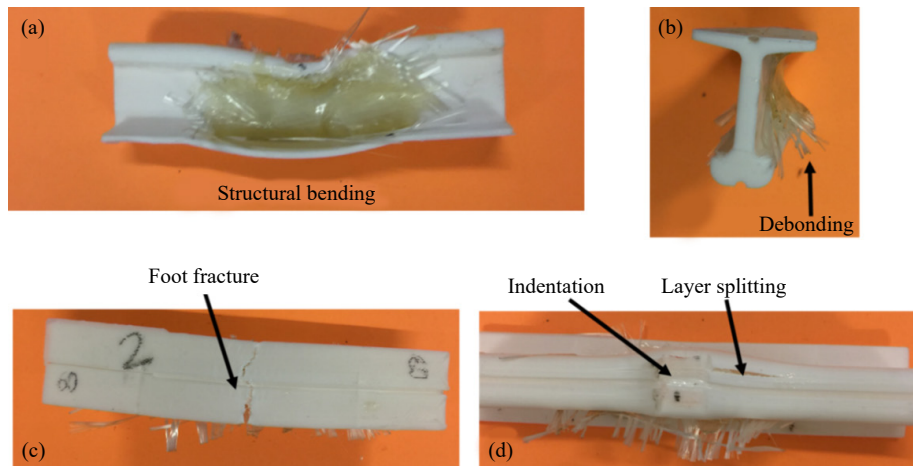


**Figure 11.** Typical failure modes: (a) structural bending; (b) debonding; (c) tensile fracture; (d) indentation and layer splitting (view from top) (Photo: Mike Hermann)

The behaviors of the 40FlexF specimen are similar to that of the 20% specimen (20FlexF) but with better-defined initial linear behaviors (Figure 10(b)). The previously described damage to the track is less obvious in this case than with its less dense counterpart. A summary here involves: the top flange indentation depth was found to be less than that of the 20FlexF specimen due to it having fewer voids; the transitions in the load-displacement curve are seen to be smoother for the 40FlexF; the failure mode at the 1st peak load was, once again, the top flange indentation; similar to the 2nd and 3rd peak loads from the 20FlexF specimen, the 40FlexF specimen also experienced web local buckling but not in as pronounced a fashion; further loading resulted in the debonding of the FRP cloth on both sides of the web; the 40FlexF specimen also showed a more pronounced structural bending capacity than that of the 20% specimens.

At higher displacements, the failure modes of 60FlexF were found to be similar to that of the 40FlexF specimen with crushing of the top flange due to loading head indentation but with less obvious web local buckling. It is visible that the web had sufficient stiffness to transfer the loading to the bottom flange resulting in significant structural bending. However, the ultimate failure was due to debonding which led to a fracturing of the bottom flange (see Figure 11(c)).

With increased PLA material percentage, there was no clear distinction between the first and second peak loads as shown in Figure 10(d) of the 80FlexF sample. In this case, no top flange indentation was observed at lower displacements. Even at higher loads, the total depth of indentation was less than the depth of indentation experienced by the 60FlexF specimens. As a result, the 80FlexF sample has structural bending characteristics similar to that of the 60FlexF specimen. In this case, the bottom flange did not experience the fracture of the 60FlexF specimen, again due to the further increases in strength realized by the use of the denser beam. More detailed discussions are presented in Section 4.3.

Finally, the 100FlexF samples showed minimal top flange indentation and had the highest bending capacities with an average of 4,198 N. Structural bending was less visible than that of 80FlexF. There was visible partial debonding near the top flange that occurred at the peak load.

To summarize, it is observed that the material failure modes (i.e., top flange indentation) dictated the tracks with fewer densities. However, after initial material failures, the FRP cloth bonded to both sides of the webs helped to enhance the capacity of the tracks. Without the GFRP cloth, the 3D-printed rail track performance would only depend on the number and orientation of the layering. Figure 4 shows an example of the checker cross-section used in the fabrication of the less dense rail tracks. With the use of GFRP cloth, the less dense samples displayed mixed modes of failure including global phenomena such as structural bending, along with localized failures such as web buckling, top flange indentation, and FRP wrap-related failures like delamination.

One of the common failure modes with the external reinforcement of structures using FRP laminates is that of the so-called face wrinkling phenomenon representing localized buckling of the composite material. As mentioned, the failure modes for the 20FlexF specimen involved indentation initially followed by web local buckling and ending, finally, in delamination. A transition was found to occur with increasing fiber content. Although the initial mode of

failure observed was still the indentation of the top flange, now, however, it was found that the mode of web local buckling was able to be circumvented due to the presence of the external GFRP cloth in that area. An actual failure mode switching was found to occur between the global modes as early as the 60FlexF specimen with the bottom flange fracture occurring at high displacements. In both the 80FlexF and 100FlexF sample cases, neither the local nor global failure modes were observed at lower displacements. The main cause of failure was partial debonding instead. A splitting of the web for the 80FlexF case occurred after the bonded layer detached. Once again, peak loading data is given in Table 2.

### 3.2 Comparison with non-reinforced specimen

To understand how the FRP wrapping may impact the flexural behavior of these 3D-printed track specimens, this section will further expound on the differences between the observed failure modes between the wrapped and unwrapped specimens. Because of the layering direction and the track densities considered, the failure modes from the load tests of unreinforced specimens ranged from localized crushing (material-controlled) failures to those dictated by bending (structurally controlled) [4]. Using flexural load tests, a transition zone between material-controlled and structural-controlled failures was observed among the specimens having between 60% to 80% PLA fiber densities. Figure 12 shows the results of the bending tests of the unreinforced samples. From Table 3, the 1st peak load of the 20% sample with fiber bonded (1,149 N) is slightly higher than its unreinforced counterpart (956 N). This increase is not very significant because the failure at the first peak loads for both the 20Flex and 20FlexF specimen cases is due to indentations of the top flanges. Hence, the addition of fiberglass to the web had little effect on the first peak for the 20% samples. However, there was a difference found in the behaviors in this region beyond the 1st peak load, in that, while the mode of failure is still localized web buckling, the load capacities were found to increase in 20% of samples due to the presence of the GFRP. The 20FlexF specimen showed layer splitting which was observed in the 20Flex specimen.

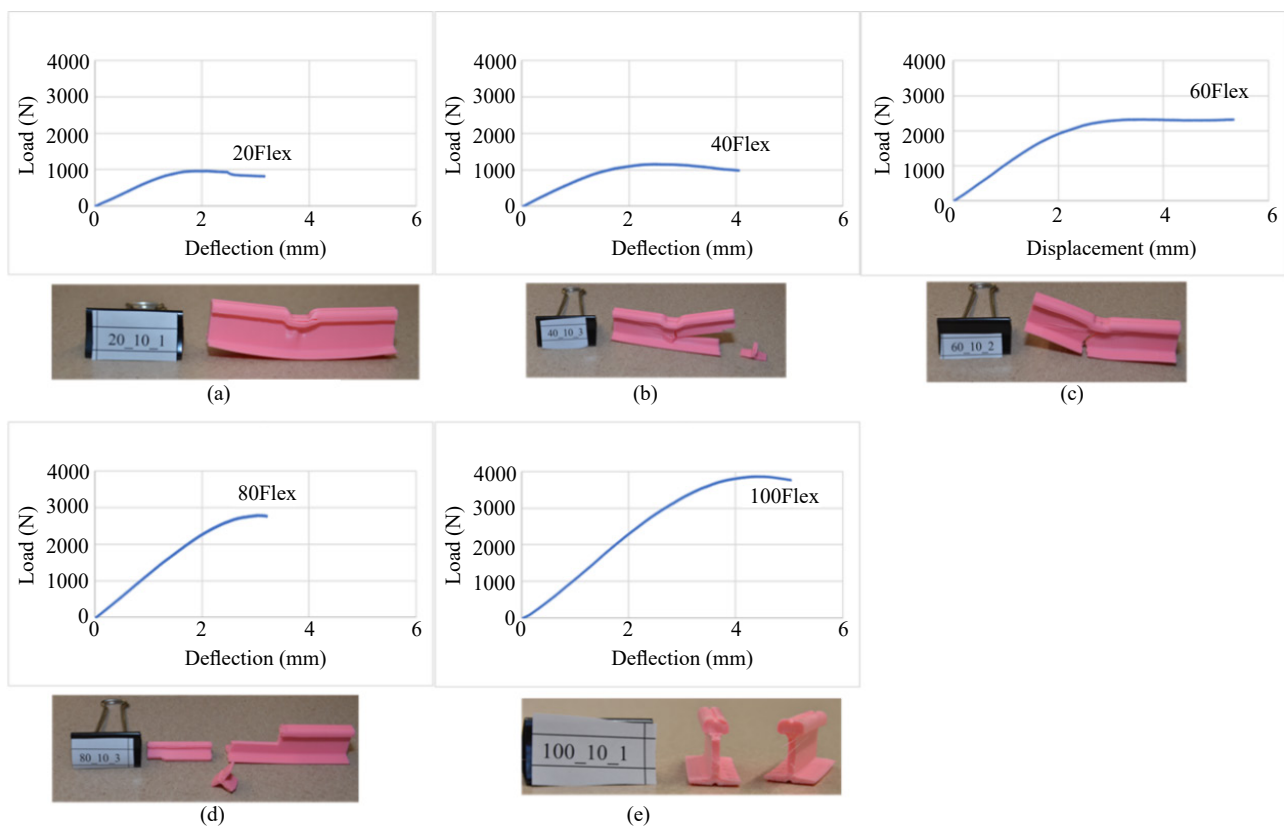


Figure 12. Load-displacement plots for non-reinforced rail track specimens with different PLA amounts: (a) 20%; (b) 40%; (c) 60%; (d) 80%; (e) 100% (photo: Mike Hermann)

**Table 3.** First peak load comparison

Specimen type	Peak load without fiber (N)	Peak load with FRP wrap (N)	Increase (N)	% Increase
20Flex	956	1,149.0	193	20.2
40Flex	1,143	1,901.1	758.1	66.3
60Flex	2,255	3,837.3	1,582.3	70.2
80Flex	2,695	4,069.9	1,374.9	51.0
100Flex	3,772	4,198.3	426.3	11.3

For the 40FlexF and 60FlexF specimens, both accommodated higher first peak loads (1,901.1 N and 3,837.3 N) when compared to their unreinforced counterparts, 40Flex (1,143 N) and 60Flex (2,255 N), representing an increase of 66% and 70%, respectively, with failure modes being similar between the two.

The causes of failure seen for the 80Flex specimens included web buckling and horizontal splitting, together with a foot fracture. The reinforced cases (80FlexF), however, did not exhibit the latter two of web horizontal splitting and foot fracture. The presence of the GFRP prevented these failure modes. This is shown in Figure 12(d) where the cause of failure of the unreinforced 80Flex cases was web horizontal splitting without foot fracture. Partial debonding occurred at the second peak load (4,035.8 N) for 80FlexF.

The structural beam fracture mode was observed in the 100Flex specimen. Although fracturing was prevented in the 100FlexF case, the specimens were seen to continuously bend with increasing displacement at a level of 9 mm after which the specimen touched the loading head at the top. From Figure 12(e), it can be seen that the beam fracture failure mode governed for the 100Flex cases at high loads. The addition of GFRP prevented the occurrence of beam fracture even for high displacements. Further loading caused bending in the specimens without splitting or splintering effects.

### 3.3 Peak load analysis

Table 3 shows the average first peak loads for the samples with different PLA densities along with the increase in bending capacity when compared to samples without GFRP cloth. As mentioned in the previous section, the 20% specimens showed about a mere 193 N (43 lb) increase in loading as the GFRP cloth on the web has no influence over indentation effects to the top flange.

The 40FlexF reinforced sample showed an increase of 758N (170 lb) when compared to the unreinforced 40Flex specimen. The failure mode was also observed to change from web buckling to top flange fiber failure. This implies that the GFRP cloth helped to prevent web local buckling. It was found that web local buckling was altogether prevented in the 60% fiber sample (60FlexF; the failure mode was still top flange indentation). The ultimate failure mode remained to be foot fracture, similar to the cases for the 60Flex specimens. The increase in bending force was also seen to peak at a load value of 1,582 N (356 lb).

The 80FlexF sample showed the second-highest bending capacity increase of 1,375 N (309 lb). Again, the bonded GFRP cloth resisted web buckling and web horizontal splitting. One of the samples showed web horizontal splitting, but it came only after the occurrence of peak loading and debonding.

Finally, the 100FlexF had the lowest percentage increase in bending capacity at 426 N (96 lb; an 11% increase). However, the addition of GFRP cloth helped to increase its stiffness.

To help better appreciate the effects of furnishing external reinforcement at the web locations in the specimens by application of the GFRP cloth, the peak load versus the fiber content curves for both the reinforced as well as the unreinforced rail tracks were plotted together (Figure 13). The plot shows the higher peak loads for the reinforced specimens. In both cases, it is observed that there is a change in peak loads between 40% and 60% fiber content specimens. Trendlines were also used in Figure 13 to help illustrate the correlations between the fiber content and first peak bending loads: A linear correlation is used for the resulting first peak bending capacity loads for the fiber reinforced specimens:

$$\text{Peak load} = 41.337 * (\% \text{Fiber}) + 550.9; R^2 = 0.864, \quad (1)$$

where  $R^2$  is the coefficient of determination.

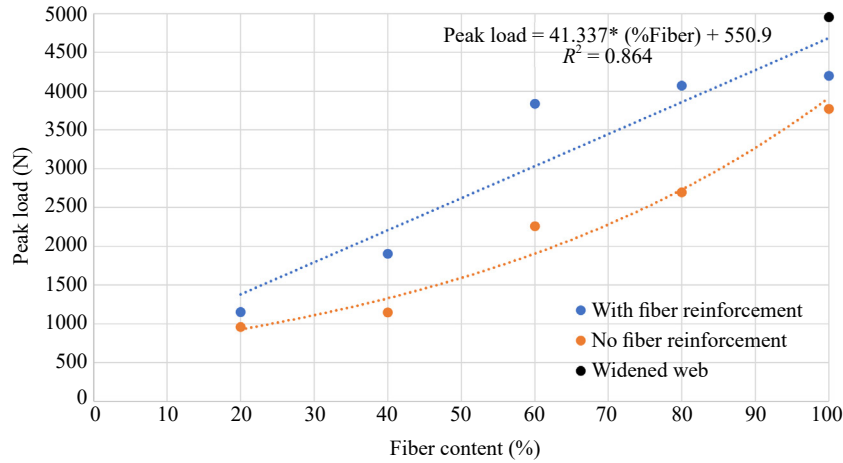


Figure 13. Peak bending load comparison

For the unreinforced specimens, a nonlinear correlation was attempted [6]. The corresponding equation and coefficient of determination are

$$\text{Peak load} = 646.15e^{0.018 * (\% \text{Fiber})}; R^2 = 0.9685. \quad (2)$$

### 3.4 Tangent stiffness calculation

The slope of the linear portion of a load-displacement graph is called the tangent stiffness which can help quantify the linear elastic behavior of a specimen. Each subfigure in Figure 12 shows such a line and the point where the load-displacement plot begins to depart from such a straight line. Figure 14 shows the change in stiffness concerning the change in the amount of PLA material content that was used for both the reinforced as well as the unreinforced specimens. It can be seen that the addition of GFRP increased the tangent stiffness of the samples. The 100FlexF showed the highest increase in strength, which helps to demonstrate the importance of the GFRP cloth. The trendlines show that the increase in tangent stiffness is found to make gains with fiber content increases which match expectations and observations of the initial stages in the loading curves.

A linear curve fit was performed for the tangent stiffness of fiberglass reinforced track versus fiber content plot which resulted in the following equation and  $R^2$  value:

$$\text{Tangent stiffness} = 10.398 * (\% \text{Fiber}) + 664.9; R^2 = 0.9753. \quad (3)$$

A power fit was done for the curve for the unreinforced tracks. The corresponding trendline equation together with the  $R^2$  value is as follows:

$$\text{Tangent stiffness} = 197.72 * (\% \text{Fiber})^{0.3888}; R^2 = 0.8372. \quad (4)$$

The high  $R^2$  value indicates that the wrapping reinforcements can brace the 3D-printed tracks with a consistent stiffening when compared to the unreinforced 3D-printed tracks. From a design perspective, a recommendation can be made by the rail design engineers to use the GFRP cloth to externally reinforce the 3D printed tracks of lesser density while maintaining adequate performance.

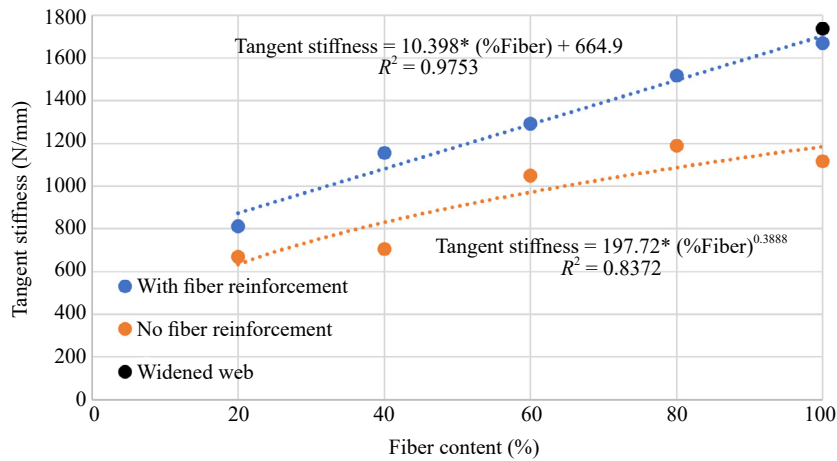


Figure 14. Tangent stiffness for different fiber content.

### 3.5 Web-widened element

To show that the web stiffening using GFRP wrapping has a similar effect as the actual widening of the web cross-section, additional 3D printed tracks (100% fiber content) were produced with the webs widened to be equal to the top flange of the railroad track. Figure 15 shows the widened web track and the bending test results of the beam. The web widening has made the track into a solid rectangular beam with an extended bottom flange. As shown, in Figure 15(b), the load test result showed that the beam failed in fracture at the bottom of the beam (tensile fracture). The load test results from three separate tests indicated that the beams with the widened web have repeatable strength of approximately 5,000 N, which is higher than the strengths of GFRP-wrapped tracks with 100% fiber contents (4,000 N). Nonetheless, the computed tangent stiffness of the web-widened track is compatible with the fiber wrap-reinforced specimens with 100% fiber contents as shown in Figure 14.

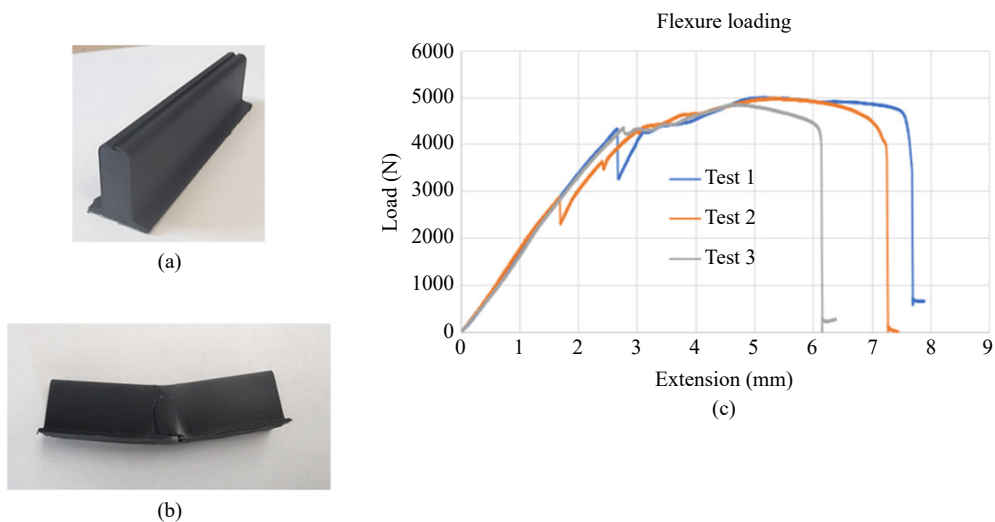


Figure 15. Web-widened element and bending test results: (a) the web-widened specimen; (b) the bending failed specimen; (c) load test results

## 4. Conclusions

To determine the effectiveness of the GFRP wrapping on additively manufactured railroad tracks for MPMs, several rail samples with varying amounts of PLA infill were fabricated using AM which were then reinforced on both sides of the web of each rail by using strips of GFRP cloth impregnated by a polyester-based resin. Three-point bending tests were then performed on the specimens and the test results showed consistent improvement of the bending capacities of the wrapped specimens. Hence, the bending capacities and failure modes of 3D printed rail tracks can vary significantly depending on the amount of infill content and whether specimens were externally reinforced with the GFRP cloth. The following observations are summarized in detail:

- a. Enhancements in the form of increased fiber contents were observed by the increases in the initial peak load capacities being attained. Specifically, for the reinforced tracks, the results showed that as the PLA content increased from 20% to 100%, the mode of failure transitioned from more localized failures to those at a global performance level. This transition occurred for infill specimens with fiber contents ranging between 40% to 60%.
- b. For the cases of the unreinforced rail track samples, the transition described in the first bullet was found to occur for fiber contents ranging between 60% to 80%. As a result, when compared to the unreinforced specimens, the reinforced 60% samples showed the highest increase in bending capacity with a peak load of 1,582 N and for the 70% fiber content sample, respectively.
- c. The tangent stiffnesses of the specimens were also calculated to see the effect of fiberglass reinforcement during small deformations. All specimens showed an increase in tangent stiffness contrasting to the unreinforced counterparts, with the 100% fiber content samples showing the highest increases in tangent stiffness.
- d. 100% fiber content specimens with web widened to the size of the top flange were also made and loaded tested and the results are shown to have higher loading capacity (5,000 N) than the GFRP wrapped tracks with 100% fiber contents (4,000 N) but with similar values of tangent stiffness.

This work represents the first experimental validation of GFRP wrapping as a means of externally reinforcing 3D-printed PLA railroad tracks. However, the hand layering technique may have introduced some experimental errors and resulted in the current load capacities. Improvement on the GFRP wrapping technique such as using VIP can improve the track strength and performance.

Future studies will include numerical analyses to provide the necessary theoretical basis for additively manufactured materials. 3D printing technology also lends itself to smart technologies such as integrating fiber optic sensors during the printing process - making rail tracks smart enough to sense changes. The feasibility of having such sensors built in during the printing process will be explored. Finally, locomotives rolling on the railroad tracks can induce significant vibration problems, which may adversely impact the GFRP wrapping scheme, which should be investigated in the future.

## Acknowledgments

The authors would like to acknowledge Mr. Mike Hermann of UNC Charlotte for his assistance in capturing the professional photographs of the tested samples shown in the figures of this study.

## Conflict of interest

There is no conflict of interest for this study.

## References

- [1] Hager I, Golonka A, Putanowicz R. 3D printing of buildings and building components as the future of sustainable construction? *Procedia Engineering*. 2016; 151: 292-299. <https://doi.org/10.1016/j.proeng.2016.07.357>

- [2] Freeman DH. Layer by layer: With 3-D printing, manufacturers can make existing products more efficiently - and create ones that weren't possible before. *MIT Technology Review*. December 19 2011. <https://www.technologyreview.com/2011/12/19/20869/layer-by-layer/> [Accessed 30th May 2023].
- [3] Camacho DD, Clayton P, O'Brien WJ, Seepersad C, Juenger M, Ferron R, et al. Applications of additive manufacturing in the construction industry—A forward-looking review. *Automation in Construction*. 2018; 89: 110-119. <https://doi.org/10.1016/j.autcon.2017.12.031>
- [4] Fu H, Kaewunruen S. State-of-the-art review on additive manufacturing technology in railway infrastructure systems. *Journal of Composites Science*. 2021; 6(1): 7. <https://doi.org/10.3390/jcs6010007>
- [5] Mortazavian E, Wang Z, Teng H. Finite element investigation of thermal-kinetic-mechanical evolutions during laser powder deposition as an innovative technique for rail repair. *The International Journal of Advanced Manufacturing Technology*. 2022; 118: 319-342. <https://doi.org/10.1007/s00170-021-07873-y>
- [6] Chen SE, Shanmugam NS, Boyajian D, Chavan VS, Weber E, Baarsons K. Prototyping rail track for micro-people movers using additive manufacturing: Failure topology characterization. *Construction and Building Materials*. 2021; 281: 122623. <https://doi.org/10.1016/j.conbuildmat.2021.122623>
- [7] Kodama H. Automatic method for fabricating a three-dimensional plastic model with photo-hardening polymer. *Review of Scientific Instruments*. 1981; 52(11): 1770-1773. <https://doi.org/10.1063/1.1136492>
- [8] Hague R, Campbell I, Dickens P. Implications on the design of rapid manufacturing. *Proceedings of the Institution of Mechanical Engineers, Part C: Journal of Mechanical Engineering Science*. 2003; 217(1): 25-30. <https://doi.org/10.1243/095440603762554587>
- [9] Labonnote N, Rønnquist A, Manum B, Rütther P. Additive construction: State-of-the-art, challenges and opportunities. *Automation in Construction*. 2016; 72: 347-366. <https://doi.org/10.1016/j.autcon.2016.08.026>
- [10] Scheithauer U, Schwarzer E, Richter HJ, Moritz T. Thermoplastic 3D printing—An additive manufacturing method for producing dense ceramics. *International Journal of Applied Ceramic Technology*. 2015; 12(1): 26-31. <https://doi.org/10.1111/ijac.12306>
- [11] Bentz DP, Jones SZ, Bentz IR, Peltz MA. Towards the formulation of robust and sustainable cementitious binders for 3D additive construction by extrusion. In: Sanjayan JG, Nazari A, Nematollahi B. (ed.) *3D Concrete Printing Technology*. Oxford, United Kingdom: Butterworth-Heinemann; 2019. p.307-331. <https://doi.org/10.1016/B978-0-12-815481-6.00015-4>
- [12] Feldmann M, Kühne R, Citarelli S, Reisgen U, Sharma R, Oster L. 3D-Drucken im Stahlbau mit dem automatisierten wire arc additive manufacturing. *Stahlbau*. 2019; 88(3): 203-213. <https://doi.org/10.1002/stab.201800029>
- [13] Leone M, Matthys S, Aiello MA. Effect of elevated service temperature on bond between FRP EBR systems and concrete. *Composites Part B: Engineering*. 2009; 40(1): 85-93. <https://doi.org/10.1016/j.compositesb.2008.06.004>
- [14] Foster SK, Bisby LA. High temperature residual properties of externally bonded FRP systems. In: Shield CK, Busel JP, Walkup SL, Gremel DD. (eds.) *SP-230: 7th International Symposium on Fiber-Reinforced (FRP) Polymer Reinforcement for Concrete Structures*. American Concrete Institute; 2005. p.1235-1252. <https://doi.org/10.14359/14891>
- [15] Canadian Standards Association (CSA). CSA Standard S806-02. *Design and construction of building components with fibre-reinforced polymers*. Toronto: CSA; 2002. [http://giacoketcau.com/download/CSA-S806-02\\_Design-and-Construction-of-Building-Components-with-Fibre-Reinforced-Polymers.pdf](http://giacoketcau.com/download/CSA-S806-02_Design-and-Construction-of-Building-Components-with-Fibre-Reinforced-Polymers.pdf)
- [16] ACI Committee 440. *Guide for the design and construction of externally bonded FRP systems for strengthening concrete structures*. American Concrete Institute. Report number: ACI PRC-4402-17, 2017.
- [17] Deniaud C, Roger Cheng JJ. Reinforced concrete T-beams strengthened in shear with fiber reinforced polymer sheets. *Journal of Composites for Construction*. 2003; 7(4): 302-310. [https://doi.org/10.1061/\(ASCE\)1090-0268\(2003\)7:4\(302\)](https://doi.org/10.1061/(ASCE)1090-0268(2003)7:4(302))
- [18] Triantafillou TC. Shear strengthening of reinforced concrete beams using epoxy-bonded FRP composites. *ACI Structural Journal*. 1998; 95: 107-115. <https://www.researchgate.net/profile/Thanasis-Triantafillou/publication/247509718>
- [19] Grace NF, Sayed GA, Soliman AK, Saleh KR. Strengthening reinforced concrete beams using fiber reinforced polymer (FRP) laminates. *ACI Structural Journal-American Concrete Institute*. 1999; 96(5): 865-874.
- [20] Stylianidis PM, Petrou MF. Study of the flexural behaviour of FRP-strengthened steel-concrete composite beams. *Structures*. 2019; 22: 124-138. <https://doi.org/10.1016/j.istruc.2019.07.012>
- [21] Gardner DJ, Davalos JF, Muniapalle UM. Adhesive bonding of pultruded fiber-reinforced plastic to wood. *Forest Products Journal*. 1994; 44(5): 62. <https://www.proquest.com/scholarly-journals/adhesive-bonding-pultruded-fiber-reinforced/docview/214637083/se-2>

- [22] Triantafillou TC. Shear reinforcement of wood using FRP materials. *Journal of Materials in Civil Engineering*. 1997; 9(2): 65-69. [https://doi.org/10.1061/\(ASCE\)0899-1561\(1997\)9:2\(65\)](https://doi.org/10.1061/(ASCE)0899-1561(1997)9:2(65))
- [23] Dempsey DD, Scott DW. Wood members strengthened with mechanically fastened FRP strips. *Journal of Composites for Construction*. 2006; 10(5): 392-398. [https://doi.org/10.1061/\(ASCE\)1090-0268\(2006\)10:5\(392\)](https://doi.org/10.1061/(ASCE)1090-0268(2006)10:5(392))
- [24] Schnerch D, Dawood M, Rizkalla S, Sumner E. Proposed design guidelines for strengthening of steel bridges with FRP materials. *Construction and Building Materials*. 2007; 21(5): 1001-1010. <https://doi.org/10.1016/j.conbuildmat.2006.03.003>
- [25] Zhao XL, Zhang L. State-of-the-art review on FRP strengthened steel structures. *Engineering Structures*. 2007; 29(8): 1808-1823. <https://doi.org/10.1016/j.engstruct.2006.10.006>
- [26] Boyajian DM, Davalos JF, Ray I. Appraisal of the novel single contoured-cantilever beam. *Materials and Structures*. 2005; 38(1): 11-16. <https://doi.org/10.1007/BF02480569>
- [27] Chajes MJ, Thomson Jr TA, Farschman CA. Durability of concrete beams externally reinforced with composite fabrics. *Construction and Building Materials*. 1995; 9(3): 141-148. [https://doi.org/10.1016/0950-0618\(95\)00006-2](https://doi.org/10.1016/0950-0618(95)00006-2)
- [28] Chen GM, Li SW, Fernando D, Liu PC, Chen JF. Full-range FRP failure behaviour in RC beams shear-strengthened with FRP wraps. *International Journal of Solids and Structures*. 2017; 125: 1-21. <https://doi.org/10.1016/j.ijsolstr.2017.07.019>
- [29] Anandan S, Dhaliwal G, Ganguly S, Chandrashekhara K. Investigation of sandwich composite failure under three-point bending: Simulation and experimental validation. *Journal of Sandwich Structures & Materials*. 2020; 22(6): 1838-1858. <https://doi.org/10.1177/1099636218791162>